Open-Source Environment for Interactive Finite Element Modeling of Optimal ICD Electrode Placement

Matthew Jolley[1], Jeroen Stinstra[3], David Weinstein[3], Steve Pieper[2], Raul San Jose Estepar[2], Gordon Kindlmann[2], Rob MacLeod[3], Dana H. Brooks[4], and John K. Triedman[1]

[1] Department of Cardiology, Children's Hospital Boston, Boston, MA
[2] Surgical Planning Laboratory, Brigham and Women's Hospital, Boston, MA
[3] Scientific Computing Institute, University of Utah, Salt Lake City, UT
[4] Department of Electrical Engineering, Northeastern University, Boston, MA
John K. Triedman, MD, Children's Hospital Boston,
300 Longwood Ave. Boston, MA 02115
john.triedman@cardio.chboston.org

Abstract. Placement of Implantable Cardiac Defibrillator (ICD) leads in children and some adults is challenging due to anatomical factors. As a result, novel *ad hoc* non-transvenous implant techniques have been employed clinically. We describe an open-source subject-specific, image-based finite element modeling software environment whose long term goal is determining optimal electrode placement in special populations of adults and children Segmented image-based finite element models of two children and one adult were created from CT scans and appropriate tissue conductivities were assigned. The environment incorporates an interactive electrode placement system with a library of clinically-based, user-configurable electrodes. Finite element models are created from the electrode poses within the torsos and the resulting electric fields, current, and voltages computed and visualized.

1 Introduction

Implantable cardiac defibrillators (ICDs) are widely used in patients at risk of fatal cardiac arrhythmias, and indications for their use continue to expand[6], [8], [9], [22]. Although ICDs are routinely implanted in adult patients using a transvenous system, there is a growing population of pediatric and adult patients in whom transvenous ICD systems cannot or should not be implanted[19]. These include very small patients and those with intracardiac shunts or anatomical obstruction to lead placement[6], [7], [10].

In these groups, several novel, non-transvenous approaches to ICD implantation have been reported (Figure 1)[7], [10], [18], [23], [24]. Such approaches have consisted of *ad hoc* adaptations of existing ICD systems, with the goals of minimizing system invasiveness, adapting to complex anatomy, and achieving low defibrillation thresholds.[7], [12], [24]. These approaches assume efficacy by extrapolation from limited animal research, and post-implantation assessment of defibrillation thresholds (DFTs)[7]. Although defibrillation research has elucidated reasonably accurate relations between distribution of myocardial voltage gradient and both defibrillation

F.B. Sachse and G. Seemann (Eds.): FIMH 2007, LNCS 4466, pp. 373–382, 2007.

efficacy and myocardial injury, no reports currently describe the effects of interactions between variations in body size and novel ICD geometries on these fields[4], [25], [27].

Animal models of defibrillation have shown defibrillation with subcutaneous electrodes to be feasible, but little is known about ideal placement or the resulting electric fields[7], [25], [27]. In the past, insertable electrodes have been used to map the epicardium and measure electric fields transmurally in animals but these techniques are expensive, time consuming and not necessarily applicable to human anatomy. Furthermore they do not provide detailed descriptions of the electric field throughout the entire myocardium and can perturb the measured fields.

Finite element modeling (FEM) of defibrillation has been shown to correlate well with clinically observed DFTs in laboriously constructed conductivity models of the adult torso[3], [11], [14], [15], [20], [21]. These studies have shown the utility of realistic models to accurately predict threshold voltages, currents, and impedances, as well as the electric fields and voltages at known measurement locations. They also may be used to compare the relative efficacy of electrode orientations in a given torso model[3], [11].

The demands of extending these studies to highly variable electrode design and placement, not to mention body size, habitus and possible gross anatomical variability, mean that such simulation systems need to allow more automatic model creation, interactive electrode placement, a wide variety of electrodes, interactive execution of the simulations, and visualization of the results. In this study, we describe the creation of an open-source subject-specific, image-based finite element modeling software environment with the goal of enabling determination of optimal electrode placement in special populations of adults and children.

2 Methods

2.1 Image Acquisition, Segmentation

Images were constructed by segmenting normal or trivially abnormal 64-detector CT scans with 1.25mm slices obtained from a radiology trauma database with appropriate IRB approvals. Of more than 50 studies examined, three patients were selected for this study based on 1) good tissue contrast, 2) minimal cardiac motion artifact, and 3) diversity of body size and habitus: a 12 kg, 2 year old female, a 32 kg, 10 year old male, and a 75 kg, 29 year old male. Torsos were segmented into 10 tissue compartments using 3D Slicer (Table 1)[1]. Various techniques were used for segmentation including thresholding, confidence connected component analysis, and level sets. The individual label maps were hierarchically combined into one label map using the unu command line tool, part of the Teem toolkit[17]. Each combined label map was imported into SCIRun/BioPSE, to solve the bioelectric field problem.[2]

2.2 Electrode Visualization and Placement

In order to allow interactive electrode placement inside a segmented 3D volume we created new functionality in the SCIRun/BIOPSE software package. We designed new modules which allow the user to interactively insert realistically shaped electrode wires and electrode cans into rendered images of the segmented volume. The shape model of the electrode can was generated by creating a triangular surface from the 2-D scanned images of the electrode and meshing the interior with tetrahedral elements based on the device's known thickness. The shape of the wire electrodes was determined interactively by specifying the length and diameter of the contact areas separately so the model was constrained to the desired shape of electrode. The 3 dimensional path of these “wires” was defined by a set of 5 user-movable spheres through which a cubic spline was fit and updated in real time. This interface proved to be sufficient for placing the wire electrodes into realistic clinical positions. A 3D tetrahedral model of the specified diameter and length was then created over the path defined by the spheres. The resulting shape of both electrodes could be adapted to closely resemble those used clinically and all could be moved interactively by the user in real time.

In order to support proper placement of electrodes, we expanded the visualization capabilities of SCIRun to render transparent 3D images of the separating surfaces between different tissue types and added in support to display three dimensional labels. We altered the way the user can interact with multiple simultaneous visualizations of the same the electrode placement so that one can look at the same situation from multiple view points.

2.3 Meshing and Finite Element Calculation

New modules were created in SCIRun/BioPSE to support local mesh refinement of hexahedral elements as well as finite element calculations on the resultant meshes.of varying element density.

Table 1. Comparison of conductivies used in this and prior FEM studies[3], [11], [14], [15], [21]

Tissue type	Current study (S/m)	Jorgenson (S/m)	DeJongh (S/m)	Mocanu (S/m)	Aguel (S/m)	Gabriel (S/m)
Bowel gas	0.0020	0.0020				
Connective Tissue	0.2200		0.2220			
Liver	0.1500	0.1486				0.3300
Kidney	0.0700					0.0700
Skeletal Muscle	0.2500	0.1429	0.2500	0.2500		
Fat	0.0500	0.0459		0.0500		
Bone	0.0060	0.0063		0.0100		
Lung	0.0670	0.0667	0.0780	0.0700	0.0500	
Blood	0.7000	0.6494	0.6670	0.8000	0.7700	
Myocardium	0.2500	0.2381	0.2500	0.2500	0.6000	

In order to create an electrical model of the torso, we combined the label maps and the electrode models described previously in a full hexahedral mesh. A regular mesh of hexahedral elements with a user adjustable spacing was created in the same space as the label map. Elements contained in a bounding box 1.5 times the 3D volume of the electrode were automatically selected and each of these elements was split into 27 smaller elements to allow for a higher local mesh density around the electrodes[26]. Using a lookup table with conductivity values (Table 1), the segmented label map was transformed into a conductivity map of the torso, whose values were projected onto the computational mesh by sampling the conductivities delineated by the label map segmentation. We assumed the electrical properties of the torso to be defined by one conductivity value per element. The resulting finite element model created by the SCIRun software resulted in a set of equations similar to those used in previous defibrillation studies[3], [11], [14]. In our implementation we assumed a linear, piecewise constant and isotropic volume conductor model, with negligible capacitance and inductance. We used the Galerkin finite element formulation with tri-linear interpolation. Electrodes were assigned a constant potential over their surface. The mesh size and spacing was interactively adjusted until additional refinements did not alter the results of the defibrillation threshold parameter by more than 1 percent. We used a representative selection of electrode positions to evaluate adequate node spacing subsequently used for each model. This resulted in a basic torso mesh that was wrapped into a grid of 100 by 100 by 150 nodes in the x, y, and z-direction, with further refinement around the electrodes as noted.

2.4 Solution Calculation, Defibrillation Metrics, and Data Analysis

After the potential distribution was solved using the finite element method, the gradients of the potential field were evaluated for the full thorax assuming a tri-linear interpolation. As the electrical field scales linearly with the potential difference applied to the defibrillation electrodes, effective electrode defibrillation potentials can be computed by linear scaling. The critical mass hypothesis was used to define successful defibrillation[12], [28]. This hypothesis proposes that defibrillation depends on rendering a critical mass of the myocardium inexcitable. A shock is predicted to be successful if it produces a threshold voltage gradient over a "large" fraction portion of the myocardial mass. Empirically determined values for these thresholds vary somewhat. The criteria used in this study of a voltage gradient of 5 V/cm generated over 95% of the myocardium has been accepted in the literature as a reasonable predictor of successful defibrillation.

Calculated metrics included the voltage, voltage gradient, current, impedance, and energy threshold (E) for defibrillation (defibrillation threshold, DFT). The DFT in this study was calculated by the energy relation $E = ½\ CV^2$, where C is the capacitance of a typical pulse generator, and V is the potential difference between electrodes required to produce a voltage gradient of 3 and 5 V/cm in 95% of the myocardium. We also calculated the percentage of myocardium above 30V/cm and 60V/cm at these thresholds, to predict possible areas of myocardial damage. We utilized a capacitance of 130uF for these estimates, based on conversations with contacts in industry. SCIRun was utilized to visualize voltage, voltage gradients, and current density. In addition the percentage of myocardium above the defibrillation threshold was calculated and visualized by projecting a color scale onto the myocardial elements.

3 Results

We utilized our newly developed functionality in SCIRun for importing segmented data, which was subsequently used in SCIRun's dataflow environment to create a computational model of the distribution of the electrical field, as shown in Figure 1(left). These dataflow networks were used for interactive placement of electrodes, remeshing of volumes around the active electrodes, calculation of FEM solutions, and presentation of data in graphs with a summary of important numerical values, as shown in figure 1(right).

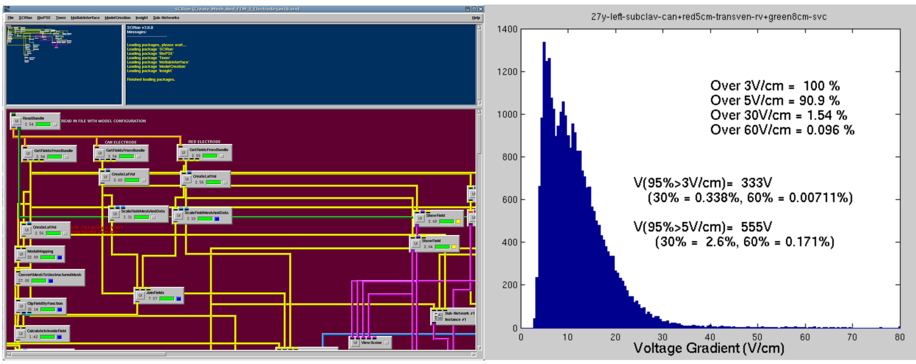

Fig. 1. SCIRUN Network: Example SCIRun Network (left) and of automatically generated numerical metrics for defibrillation (right) for a standard adult transvenous electrode configuration with a shock of 500V as well as scaled metrics

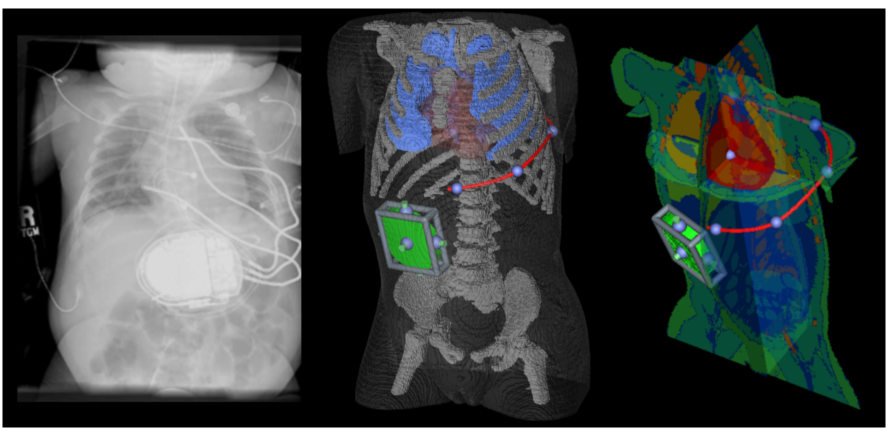

Fig. 2. Subcutaneous Electrode placement: Left: Chest x-ray of subcutaneous electrode placement in child. Middle: Example of subcutaneous electrode placement in 2-yr old model. Right: Moveable cutting planes to examine detail. Blue spheres are user moveable handles.

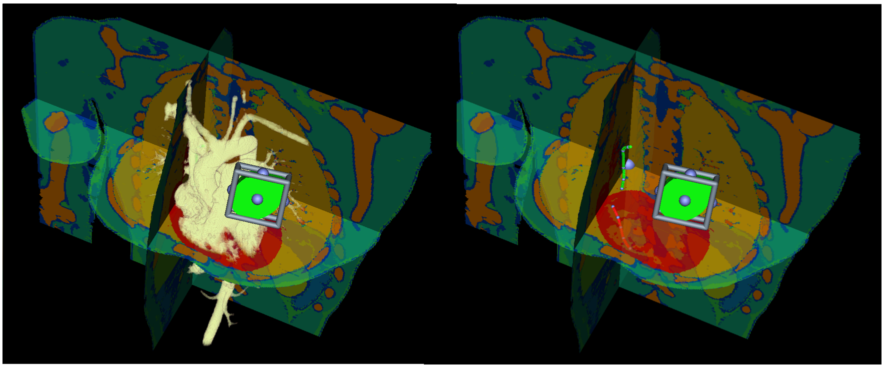

Fig. 3. Transvenous Electrode Placement: Standard adult placement with left subclavian can, 8cm coil in superior vena cava (green) and 5 cm coil in right ventricle(red) shown with (left) and without (right) rendering of blood within the 29 year old torso shown with three moveable cutting planes

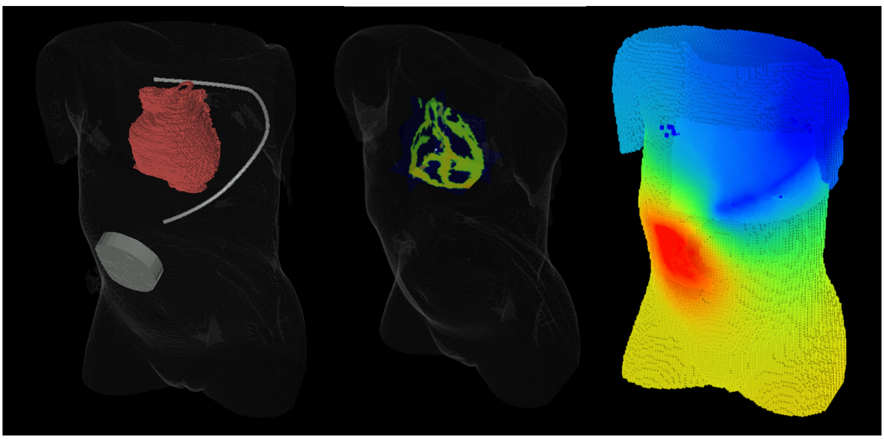

Fig. 4. Visualization of defibrillation: 2 year old child with left thoracic subcutaneous electrode and right abdominal can. Left: Electrode positions and heart within torso. Middle: Visualization of voltage gradients within the heart with three moveable cutting planes for exploration. Right: Visualization of absolute voltages on torso of model, note increased mesh density around electrodes.

Graphical representations of sample FEM solutions are shown in Figure 4 demonstrating the ability to visualize voltage gradient distribution within the myocardium as well as compute voltage and energy parameters necessary to meet the criteria of the critical mass hypothesis.

To validate our model, we compared the DFTs obtained in our 75kg adult-sized torso with standard, transvenous electrode placement to previously published adult FEM models of defibrillation[3], [11]. The calculated DFT values for our torso using standard electrode orientation are in close agreement with these models [8-12 joules, 5V/cm metric] as well as empiric clinical values.

In order to explore the clinical relevance of this newly created functionality for novel non-transvenous orientations we analyzed several exemplary situations. Clinicians have begun to use scenarios with an abdominal can and single subcutaneous 25cm electrode coil as suggested in figure 4. The best positioning of this combination and effect of small changes in electrode movement is unknown. To explore the utility of the newly created environment utilized the 2year-12kg torso and the can in the left abdomen at the level of thoracic vertebrae 12. We then extended the 25cm subcutaneous electrode to the left from the can to different locations, placing it at the level of thoracic vertebrae 6, 8, and 10 respectively. The voltage difference required to achieve 3V/cm varied from 335 volts to 654 volts, corresponding to a change in work from 7.29 joules to 27.8 joules, with the electrodes placed caudally at T6 achieving the lowest defibrillation threshold. Thus, very small changes in electrode placement in these novel configurations are predicted to have significant effect on clinical DFTs.

To compare the efficiency of the best subcutaneous orientation to a standard transvenous orientation in the 2 year old torso model we placed the can in the right and left abdomen, as well as the right and left subclavian positions, and placed a single 5cm long transvenous electrode with a diameter of 3mm in the right ventricle. The required voltage varied from 58.6 volts to 172 volts, corresponding to 0.22 and 1.92 Joules respectively, with the left subclavian can being the most efficient. In situations where it is anatomically viable and safe, standard transvenous placement of electrodes is more efficient than most subcutaneous electrode placement.

To explore the effect of body size and growth we compared the single retrocardiac electrode with an abdominal can, another orientation utilized clinically in small children, to assess the efficacy of this orientation with growth. A right abdominal can with a 5 cm electrode placed in the posterior epicardial region approximately centered in relation to the heart required 266V, 850V, and 1690V in the 2year-12kg, 10year-32kg, and 29 year-75kg torsos respectively. This corresponds to a range of approximately 3 to 185 joules expected with growth, suggesting orientations practical in one age group might fail with time.

4 Discussion

Utilization of ICD therapy in pediatric and congenital heart populations has risen, as the numbers of patients who may benefit have increased while apparent risks have decreased. Transvenous implantation often cannot be performed in children due to patient size, lack of vascular access and increased risk of embolic phenomena due to intracardiac shunts[16], [19]. Children with ICDs have high rates both of lead failure and of vascular occlusion[5], [6] and long life expectancy, resulting in the anticipated need for repeated lead extraction and reimplantation with their attendant risks. There is also growing interest in the development of extracardiac ICDs for the adult population, both to avoid lead related complications and for patients with vascular access problems or other contraindications to transvenous implant. We have utilized existing open-source tools and developed new, interactive functionality in SCIRun/BioPSE to study this problem using subject-specific FEMs and demonstrated its application.

We utilized the interactive electrode placement system to explore several clinical situations and analyze the effect of electrode placement in a given torso. A four rib change in subcutaneous electrode position is predicted to triple the DFT in Joules in a two year old torso. Transvenous electrode placement is predicted to be more efficient than subcutaneous placements, suggesting these orientation should be utilized in patients with suitable anatomy. Retrocardiac placement of a single electrode to an abdominal can is a reasonable orientation in a small child, but not in a older child or adult as the resulting DFTs are in excess of what current devices can deliver. Together these examples suggest that the rapidly adaptable environment we have created will be potentially useful in designing optimal electrode placements in children and adults with unique anatomy and other technical requirements.

Previous publications have shown that FEM can closely correlate with clinically observed results[3], [11], [13], [15]. Although this is reassuring, both the current and prior models do not incorporate many factors known to affect defibrillation. These include patient specific differences in conductivity, myocardial tissue structure, capacitive effects, the complexities of fibrillation wavefront behavior, and the effects of biphasic waveforms on membrane repolarization. Although results predicted by the critical mass hypothesis compare favorably to clinical observation, it is a gross model that largely ignores cellular level effects and does not account for variability in susceptibility of a given patient's myocardium. We expect these models to provide a platform for reasonable comparison of relative efficacies of electrode position for a given torso, and as such can serve as a useful tool for comparing novel configurations to proven electrode positions as well as general trends in comparison of different torso models. Practical application of this approach is limited at present by the availability of high resolution CT and MRI scans of children. As such scans obtained for clinical reasons will provide opportunity for further development of trends across age groups and anatomy. We plan to utilize the system to systematically explore various parameters and orientations in children and adults to better guide practitioners in situations when novel implantations are needed. We have also begun to utilize the system in a case specific manner with dedicated scans in patients with highly complicated congenital heart disease and other congenital anomalies to assess the utility of determining optimal orientations on a case by case basis.

We hope to continue to improve the tools in this open-source pipeline. Segmentation remains time intensive despite improvements in segmentation algorithms and we are actively working to create atlas based segmentation systems such that imaging can be rapidly converted to highly accurate torso models with minimal user input. The newly developed functionality in SCIRun will be improved. to be more efficient and incorporate other physically relevant parameters, and a broader library of electodes. SCIRun also has powerful visualization capabilities, and we are further exploring optimal parameters for improved perception of visual and numerical data. Once optimized the platform may be wrapped into a stand alone open source program once we are satisfied with visualization and simulation performance.

5 Conclusion

We have developed an interactive computational and visualization tool that can be used to assess the relative efficiency of non-standard ICD electrode placement in torso models of various sizes. In patients with contraindications to standard approaches to ICD implantation, the ability to interactively assess the relative efficacy of different electrode orientations may provide insight into which orientation might be optimal in a specific patient. This image-based approach may also be of value in the design and development of extracardiac defibrillation strategies.

Acknowledgements. This work was supported by NIH P41 RR12557, NIH P41 RR12553-02 , NIH P41 RR1318, NIH U54 EB005149, NIH T32 HL07572 and a Fast Forward Grant from CIMIT.

References

1. 3D Slicer: Medical Visualization and Processing Environment for Research (2004)
2. SCIRun: A Scientific Computing Problem Solving Environment (2002)
3. Aguel, F., Eason, J.C., Trayanova, N.A. et al.: Impact of Transvenous Lead Position on Active-can ICD Defibrillation: A Computer Simulation Study. PACE, 22 p.158 (1999)
4. Alcott, G., Hunter, F., Ideker, R.: Principles of defibrillation: Cellular physiology to fields and waveforms. Clinical Cardiac Pacing and Defibrillation. 2nd edn. Saunders, Philadelphia (2000)
5. Alexander, M.E., Cecchin, F., Walsh, E.P., et al.: Implications of Implantable Cardioverter Defibrillator Therapy in Congenital Heart Disease and Pediatrics. J. Cardiovasc. Electrophysiol. 15, 72 (2004)
6. Bar-Cohen, Y., Berul, C.I., Alexander, M.E., et al.: Age, Size, and Lead Factors Alone do Not Predict Venous Obstruction in Children and Young Adults with Transvenous Lead Systems. J. Cardiovasc. Electrophysiol. 17, 754 (2006)
7. Berul, C.I., Triedman, J.K., Forbess, J., et al.: Minimally Invasive Cardioverter Defibrillator Implantation for Children: An Animal Model and Pediatric Case Report. PACE 24, 1789 (2001)
8. Bokhari, F., Newman, D., Greene, M., et al.: Long-Term Comparison of the Implantable Cardioverter Defibrillator Versus Amiodarone: Eleven-Year Follow-Up of a Subset of Patients in the Canadian Implantable Defibrillator Study (CIDS). Circulation 110, 112 (2004)
9. Buxton, A.E., Lee, K.L., Fisher, J.D., et al.: A Randomized Study of the Prevention of Sudden Death in Patients with Coronary Artery Disease. Multicenter Unsustained Tachycardia Trial Investigators. The New Eng. J. Med. 341, 1882 (1999)
10. Cannon, B.C., Friedman, R.A., Fenrich, A.L., et al.: Innovative Techniques for Placement of Implantable Cardioverter-Defibrillator Leads in Patients with Limited Venous Access to the Heart. PACE 29, 181 (2006)
11. de Jongh, A.L., Entcheva, E.G., Replogle, J.A., et al.: Defibrillation Efficacy of Different Electrode Placements in a Human Thorax Model. PACE 22, 152 (1999)
12. Frazier, D.W., Wolf, P.D., Wharton, J.M., et al.: Stimulus-Induced Critical Point. Mechanism for Electrical Initiation of Reentry in Normal Canine Myocardium. J. Clin Invest 83, 1039–1052 (1989)
13. Gold, M.R., Olsovsky, M.R., DeGroot, P.J., et al.: Optimization of Transvenous Coil Position for Active can Defibrillation Thresholds. J. Cardiovasc. Electrophysiol. 11, 25 (2000)

14. Jorgenson, D.B., Haynor, D.R., Bardy, G.H., et al.: Computational Studies of Transthoracic and Transvenous Defibrillation in a Detailed 3-D Human Thorax Model. IEEE Trans. Biol. Engin. 42, 172 (1995)
15. Jorgenson, D.B., Schimpf, P.H., Shen, I., et al.: Predicting Cardiothoracic Voltages during High Energy Shocks: Methodology and Comparison of Experimental to Finite Element Model Data. IEEE Trans. Biol. Engin. 42, 559 (1995)
16. Khairy, P., Landzberg, M.J., Gatzoulis, M.A., et al.: Transvenous Pacing Leads and Systemic Thromboemboli in Patients with Intracardiac Shunts: A Multicenter Study. Circulation 113, 2391–2397 (2006)
17. Kindlmann, G.: TEEM: Tools to Process and Visualize Scientific Data and Images (2005)
18. Kriebel, T., Ruschewski, W., Paul, T.: Implantation of an “Extracardiac” Internal Cardioverter Defibrillator in a 6-Month-Old Infant. Zeitschrift fur Kardiologie 94, 415 (2005)
19. Kugler, J.D., Erickson, C.C.: Nontransvenous Implantable Cardioverter Defibrillator Systems: Not just for Small Pediatric Patients. J. Cardiovasc. Electrophysiol. 17, 47 (2006)
20. Mocanu, D., Kettenbach, J., Sweeney, M.O. et al.: A Comparison of Biventricular and Conventional Transvenous Defibrillation: A Computational Study using Patient Derived Models. PACE 27, 586 (2004)
21. Mocanu, D., Kettenbach, J., Sweeney, M.O., et al.: Patient-Specific Computational Analysis of Transvenous Defibrillation: A Comparison to Clinical Metrics in Humans. Ann. Biomed. Engin. 32, 775 (2004)
22. Moss, A.J., Hall, W.J., Cannom, D.S., et al.: Improved Survival with an Implanted Defibrillator in Patients with Coronary Disease at High Risk for Ventricular Arrhythmia. Multicenter Automatic Defibrillator Implantation Trial Investigators. The. New. Eng. J. Med. 335, 1933 (1996)
23. Schreiber, C., Eicken, A.: Nonthoracotomy Cardioverter Defibrillator Implantation in Infants. Resuscitation 69, 350 (2006)
24. Stephenson, E.A., Batra, A.S., Knilans, T.K., et al.: A Multicenter Experience with Novel Implantable Cardioverter Defibrillator Configurations in the Pediatric and Congenital Heart Disease Population. J. Cardiovasc. Electrophysiol. 17, 41 (2006)
25. Tang, A.S., Wolf, P.D., Afework, Y., et al.: Three-Dimensional Potential Gradient Fields Generated by Intracardiac Catheter and Cutaneous Patch Electrodes. Circulation 85, 1857–1864 (1992)
26. Zhang, Y., Bajaj, C.: Adaptive and Quality quadrilateral/hexahedral Meshing from Volumetric Data. Computation Methods in Applied Mechanical Engineering 195, 942–960 (2006)
27. Zhou, X., Daubert, J.P., Wolf, P.D. et al.: Epicardial Mapping of Ventricular Defibrillation with Monophasic and Biphasic Shocks in Dogs. Circ Res. 72, 145–160 (1993)
28. Zipes, D.P., Fischer, J., King, R.M., et al.: Termination of Ventricular Fibrillation in Dogs by Depolarizing a Critical Amount of Myocardium. Am. J. Cardio. 36, 37 (1975)